Journal of Nuclear Materials 405 (2010) 156–159

Contents lists available at ScienceDirect

Journal of Nuclear Materials

journal homepage: www.elsevier.com/locate/jnucmat

Development of a pair potential for Fe–He by lattice inversion

P.H. Chen [a,*], X.C. Lai [a], K.Z. Liu [a], X.L. Wang [a], B. Bai [a], B.Y. Ao [a], Y. Long [b]

[a] Science and Technology on Surface Physics and Chemistry Laboratory, Mianyang 621907, PR China
[b] Institute of Applied Physics and Computational Mathematics, P.O. Box 8009, Beijing 100088, PR China

ARTICLE INFO

Article history:
Received 15 May 2010
Accepted 6 August 2010

ABSTRACT

A new pair potential for helium in bulk iron was developed using a method based on the Chen–Möbius lattice inversion in order to study the effect of He in irradiated iron. By means of molecular dynamic (MD), we have examined this interatomic potential. Comparing with the *ab initio* calculation results, the stability of He-vacancy clusters at zero temperature and migration energy was well reproduced by this potential.

1. Introduction

Ferritic steels are possible structural materials for future fusion reactors, materials are subjected to 14 MeV neutron irradiation, generating helium by transmutation reactions and simultaneously energetic displacement damage. Helium plays a significant role in microstructural evolution and mechanical properties degradation [1,2]. However, many important effects of helium are not easily available for experimental study due to helium's high mobility via an interstitial migration mechanism and its strong binding with vacancies. Although these properties could be obtained from *ab initio* calculation, it is very costly for large-scale simulation, especially for the systems containing more than hundreds of atoms. Applying *ab initio* data to construct an empirical potential for use in classical molecular dynamics seems to be the most practical approach currently available to study He behavior in metals on the desired scale [3]. It has been suggested that a pair potentials is enough to describe simple He defects and migration of He in iron, since helium is a close-shell atom [4,5]. As a pair potential is computationally faster than a many-body potential, it is advisable to use a pair potential when it is sufficient.

In most of the previous work [3–5], the interatomic potentials were started from the selection of interatomic potential function forms with adjustable parameters, and then the potential parameters were obtained by fitting to the experimental data or calculation results, such as lattice parameters, lattice energy, phonon frequencies, and elastic properties. These potentials have played a significant role in previous simulation, especially for the materials with lots of experimental data [6–8]. However, for the metal-He interatomic potential whose properties are hard to obtain, it is hard to determine which set of potentials is the most appropriate. One of the effective solutions for the uncertainty of multiple-parameter fittings may be the lattice inversion method, which was first presented to determine the pair potentials from the *ab initio* calculated or experimentally measured adhesive energy by Carlsson, Gelatt, and Ehrenreich (CGE) [9], and then Chen used the Möbius-inversion formula in number theory to obtain the pair potentials for the pure metals with faster convergence than the CGE method [10,11].

In this paper a method [12] based on the Chen–Möbius lattice inversion was used to derive Fe–He interatomic potential. First, we constructed the extended phase space including B1 (rocksalt) and B3 structures (Fig. 1). The aim was to derive the proper interatomic potentials from an extended phase space including equilibrium and nonequilibrium states. This could cover more configurations and interatomic spacing of our interest than that only from one equilibrium configuration. Second, the pseudopotential total-energy calculations for two-type FeHe crystals were performed from lattice constant $\alpha = 0.4 - 0.86$ nm. Finally, the pair potential curves were directly evaluated from a series of the total-energy difference based on Chen–Möbius lattice inversion techniques [10,11]. Then the suitable function forms were selected to fit the pair potential curves. Furthermore, the inverted pair potential was used to describe the formation and migration of He in iron.

2. Computational models

2.1. Total-energy calculation for B1-, B3-type FeHe

According to lattice inversion [10,11], in order to extract the Fe–He pair potential, we calculated the pseudopotential total-energy of FeHe in the B1 and B3 structures with lattice constants α from 0.4 to 0.86 nm. These calculations were performed using the Vienna *ab initio* simulation package (VASP) [13–15]. Exchange and correlation are treated in the GGA with the function of Perdew and

* Corresponding author. Tel.: +86 08163626968; fax: +86 08163626738.
E-mail address: chenph@live.cn (P.H. Chen).

0022-3115/$ - see front matter © 2010 Elsevier B.V. All rights reserved.
doi:10.1016/j.jnucmat.2010.08.006

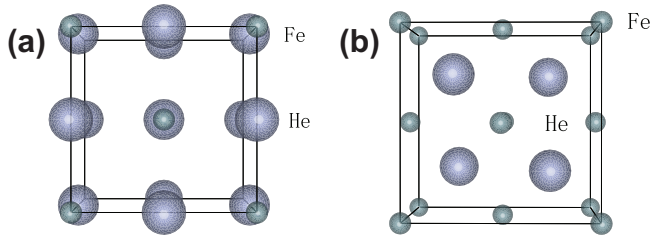

Fig. 1. Virtual structures used for *ab initio* pseudopotential total-energy calculations. (a) B1 (rocksalt) structure and (b) B3 (zinc blende) structure.

Wang (PW91) [16]. The K-mesh points over the Brillouin Zone are generated with parameters $7 \times 7 \times 7$ for the largest reciprocal space and $3 \times 3 \times 3$ for the smallest reciprocal space by the Monkhorst–Pack scheme [17]. The energy tolerance for self-consistent-field (SCF) convergence is 10^{-5} eV/atom with the plane ware energy cutoff of 550 eV. The total energies as a function of lattice constant α are shown in Fig. 2.

2.2. Chen–Möbius lattice inversion

With the identical lattice constant α, the difference between B1 and B3 structures is only about the Fe–He distance. Then the total-energy difference $E_{B1} - E_{B3}$ between B1 and B3 only depends on the Fe–He interaction, and can be rewritten as:

$$E_{B1} - E_{B3} = \frac{1}{2}\left(\sum_{B1}\phi_{FeHe}(r_{ij}) - \sum_{B3}\phi_{FeHe}(r_{ij})\right). \quad (1)$$

where ϕ_{FeHe} is the Fe–He pair potential and r_{ij} is the separation between atoms at lattice site i and j ($i \neq j$). For the B1-type FeHe, the Fe–He interaction can be expressed as

$$E^{B1}_{Fe-He}(\alpha) = \frac{1}{2}\sum_{i,j,k}\phi_{Fe-He} \times \left(\sqrt{(i+k-1)^2 + (i+j-1)^2 + (j+k-1)^2}\,\frac{\alpha}{2}\right). \quad (2)$$

where the i, j, k indicate the atomic sites of atoms in the unit of the lattice constant α. In the B3-FeHe, the Fe–He interaction is

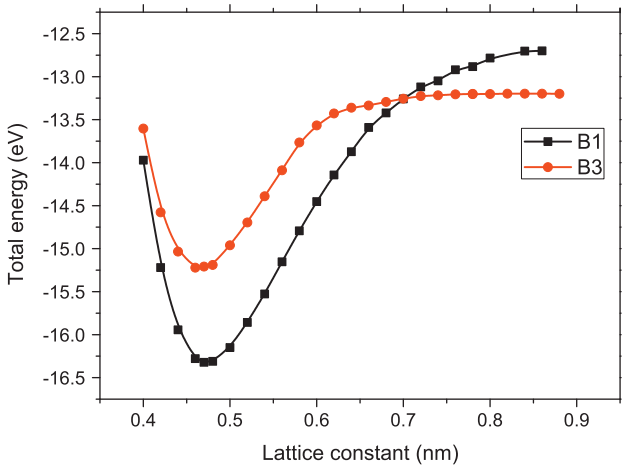

Fig. 2. Total energy versus lattice constant α of the FeHe polymorph from the VASP calculation.

$$E^{B3}_{Fe-He}(a) = \frac{1}{2}\sum_{i,j,k}\phi_{Fe-He} \times \left(\sqrt{\left(i+k-\frac{1}{2}\right)^2 + \left(i+j-\frac{1}{2}\right)^2 + \left(j+k-\frac{1}{2}\right)^2}\,\frac{\alpha}{2}\right). \quad (3)$$

Then ϕ_{FeHe} can be solved from Eqs. (1)–(3) by Chen–Möbius lattice inversion [10,11]. The pair potential was fit using a polynomial function:

$$f(r_{ij}) = \begin{cases} p1_1 r_{ij}^{10} + p1_2 r_{ij}^{9} + p1_3 r_{ij}^{8} + \cdots p1_9 r_{ij}^{2} + p1_{10} r_{ij}^{1} + p1_{11}, \\ \quad 0.01 < r_{ij} < 0.05 \\ p2_1 r_{ij}^{10} + p2_2 r_{ij}^{9} + p2_3 r_{ij}^{8} + \cdots p2_9 r_{ij}^{2} + p2_{10} r_{ij}^{1} + p2_{11}, \\ \quad 0.05 < r_{ij} < 0.1 \\ p3_1 r_{ij}^{10} + p3_2 r_{ij}^{9} + p3_3 r_{ij}^{8} + \cdots p3_9 r_{ij}^{2} + p3_{10} r_{ij}^{1} + p3_{11}, \\ \quad 0.1 < r_{ij} < 0.2 \\ p4_1 r_{ij}^{10} + p4_2 r_{ij}^{9} + p4_3 r_{ij}^{8} + \cdots p4_9 r_{ij}^{2} + p4_{10} r_{ij}^{1} + p4_{11}, \\ \quad 0.2 < r_{ij} < 0.3 \\ p5_1 r_{ij}^{10} + p5_2 r_{ij}^{9} + p5_3 r_{ij}^{8} + \cdots p5_9 r_{ij}^{2} + p5_{10} r_{ij}^{1} + p5_{11} \\ \quad 0.3 < r_{ij} \end{cases} \quad (4)$$

The final potential parameters are listed in Table 1.

Fig. 3 also shows the discrepancy among our pair potential, Wilson's potential [4], Seletskaia's potential [20] and Juslin's potential [5]. Their discrepancy lies mainly in the part of small interatomic distances, where the repulsive wall is stiffer for the Wilson's potential in comparison to the Juslin's and our potential.

3. Results and discussion

Using the above Fe–He pair potential from multiple-lattice inversion, we calculated the elastic properties of the two FeHe crystals. The first important information we can deduce from the results is the Cauchy pressure, which provides a test of the pairwise hypothesis. To describe the Fe–Fe interactions, the potential developed by Ackland et al. [18] are employed, which is generally considered to be good at describing defects and radiation damage. The He–He interactions are described using the Aziz potential [19]. The obtained C_{ij} values are given in Table 2. The Cauchy pressures calculated with the new potential for Fe–He and a many-body potential for Fe–Fe agree with DFT results. Therefore, the three-body forces for Fe–He are most likely to be very small because that He is a closed-shell atom.

The formation energies of helium interstitials in iron for substitutional, octahedral and tetrahedral positions was calculated using the classical molecular statics (MS) technique. All simulations were performed for 2000 atoms in pure bulk, adding and removing atoms at needed for the defects. The time step was 2×10^{-16} s and $r_{cutoff} = 1$ nm. The result are presented in Table 3. In Table 3 one can see that our potential reproduces the preference order for a single He defect. Comparing with the potential by Juslin et al. [5] and Seletskaia et al. [20], the formation energies of our potential are closer to DFT results.

The new Fe–He potential was then used to study the properties of He-vacancy clusters at 0 K. The dependence of the binding energy of additional He atoms to a He-vacancy cluster (substitutional He) were investigated as a function of cluster size. Firstly, helium atoms were introduced randomly in the vicinity of a vacancy site. The system was subsequently relaxed at 700 K for 10 ps, then cooled down and quenched to 0 K. To ensure the cluster obtained in this way is stable, several checks were made. That is, the orientation of the stable cluster was rotated 30° and 60°, respectively,

Table 1
Fe–He pair potential parameters obtained in this work.

$p1_1$ (eV/nm^{10})	$p2_1$ (eV/nm^{10})	$p3_1$ (eV/nm^{10})	$p4_1$ (eV/nm^{10})	$p5_1$ (eV/nm^{10})
1.143E20	3.841E15	1.497E12	6.401E8	1.955E3
$p1_2$ (eV/nm^9)	$p2_2$ (eV/nm^9)	$p3_2$ (eV/nm^9)	$p4_2$ (eV/nm^9)	$p5_2$ (eV/nm^9)
−4.861E19	−3.521E15	−2.545E12	−1.728E9	−1.294E4
$p1_3$ (eV/nm^8)	$p2_3$ (eV/nm^8)	$p3_3$ (eV/nm^8)	$p4_3$ (eV/nm^8)	$p5_3$ (eV/nm^8)
9.189E18	1.458E15	1.949E12	2.099E9	3.833E4
$p1_4$ (eV/nm^7)	$p2_4$ (eV/nm^7)	$p3_4$ (eV/nm^7)	$p4_4$ (eV/nm^7)	$p5_4$ (eV/nm^7)
−1.017E18	−3.595E14	−8.857E11	−1.510E9	−6.699E4
$p1_5$ (eV/nm^6)	$p2_5$ (eV/nm^6)	$p3_5$ (eV/nm^6)	$p4_5$ (eV/nm^6)	$p5_5$ (eV/nm^6)
7.312E16	5.859E13	2.649E11	7.126E8	7.649E4
$p1_6$ (eV/nm^5)	$p2_6$ (eV/nm^5)	$p3_6$ (eV/nm^5)	$p4_6$ (eV/nm^5)	$p5_6$ (eV/nm^5)
−3.573E15	−6.612E12	−5.453E10	−2.304E8	−5.968E4
$p1_7$ (eV/nm^4)	$p2_7$ (eV/nm^4)	$p3_7$ (eV/nm^4)	$p4_7$ (eV/nm^4)	$p5_7$ (eV/nm^4)
1.208E14	5.250E11	7.836E9	5.168E7	3.224E4
$p1_8$ (eV/nm^3)	$p2_8$ (eV/nm^3)	$p3_8$ (eV/nm^3)	$p4_8$ (eV/nm^3)	$p5_8$ (eV/nm^3)
−2.807E12	−2.911E10	−7.776E8	−7.933E6	−1.192E4
$p1_9$ (eV/nm^2)	$p2_9$ (eV/nm^2)	$p3_9$ (eV/nm^2)	$p4_9$ (eV/nm^2)	$p5_9$ (eV/nm^2)
4.354E10	1.085E9	5.110E7	7.970E5	2.886E3
$p1_{10}$ (eV/nm)	$p2_{10}$ (eV/nm)	$p3_{10}$ (eV/nm)	$p4_{10}$ (eV/nm)	$p5_{10}$ (eV/nm)
−4.166E8	−2.480E7	−2.013E6	−3.730E4	−4.138E2
$p1_{11}$ (eV)	$p2_{11}$ (eV)	$p3_{11}$ (eV)	$p4_{11}$ (eV)	$p5_{11}$ (eV)
1.951E6	2.670E5	3.621E4	1.260E3	2.670E1

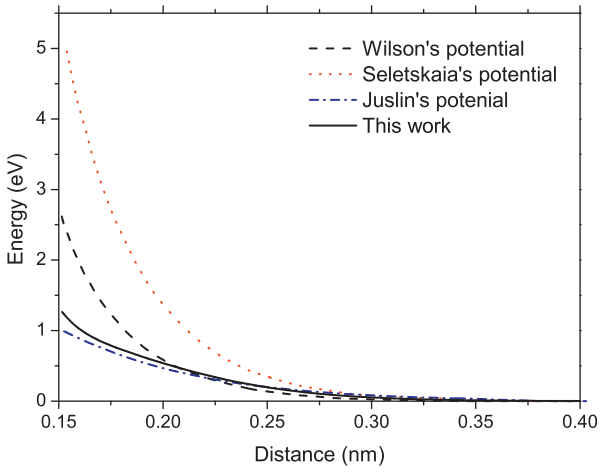

Fig. 3. Our potential, Wilson's potential [4], Seletskaia's potential [20] and Juslin's potential [5] as a function of interatomic distance.

Table 2
Calculated values for elastic constant (C_{ij} in GPa), bluk modulus (B in GPa), and Cauchy pressure (C' in GPa).

B1	B	C_{11}	C_{12}	C_{44}	C'
DFT	95	146	70	25	22.5
MD	110	181	75	27	24
B3	B	C_{11}	C_{12}	C_{44}	C'
DFT	12	16	10	−26	18
MD	21	25	20	−21	20.5

Table 3
Formation energies (eV) of helium interstitials in iron for substitutional, octahedral and tetrahedral positions.

		Substitutional	Octahedral	Tetrahedral
DFT	Seletskaia et al. [21]	3.84	4.60	4.37
MD	Wilson [22]	3.25	5.25	5.34
MD	Juslin et al. [5]	4.10	4.51	4.39
MD	Seletskaia et al. [20]	3.91	4.54	4.50
	This work	3.87	4.57	4.45

and then was processed by the quenched annealing. We find that the formation energies of the rotated clusters have almost no difference from the original stable cluster. The atomic coordinates were relaxed using a conjugate-gradient method to zero force at constant volume. The results for He atom are presented in Fig. 4. The new potential somewhat underestimates the binding energies of additional He atoms to the He-vacancy cluster. The binding energy initially decreases and then increases, with a local maximum when a total of six He atoms are involved. In this case, the cluster have relative high symmetry, e.g. He_6V_1 (one Fe atoms out and put six He in) is octahedron. Their formation energy per atom is relatively low. Thus it is difficult to deprive a He atom from the low-energy cluster to break the high symmetry. However, it becomes very easy to remove an additional He atom from a high-energy cluster to obtain the stable configuration with high symmetry. When the seventh He atoms is added to the He-vacancy cluster, it is ejected to an interstitial position. This leads to the decrease in binding energy when the seventh He atom is added [3].

Concerning the kinetics of He in bcc iron, we examine the case of interstitial He migration, which is relevant to the initial stage after He implantation or He production by transmutation. There are two most common methods to calculate the migration barrier, the nudged elastic band method [23] and the drag method [24].

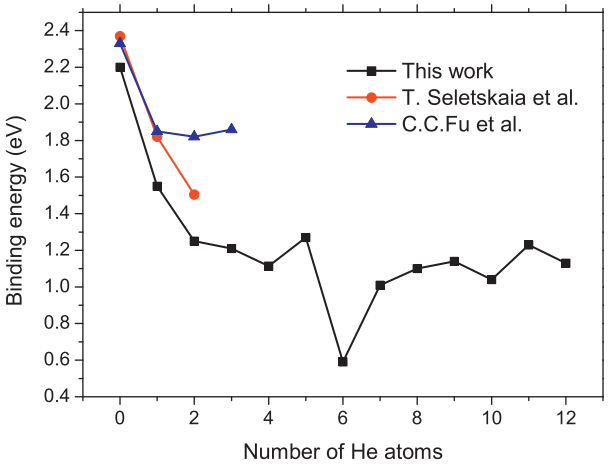

Fig. 4. Binding energy of additional He atoms to a substitutional He.

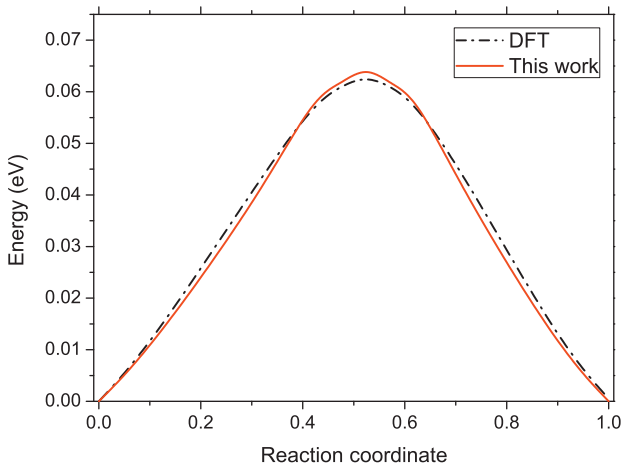

Fig. 5. The migration barrier for migration of helium in iron from one tetrahedral interstitial position to a neighboring tetrahedral position.

As the drag method was used in the DFT calculations [22], we calculated the migration of a tetrahedral interstitial He to a neighboring tetrahedral position using the drag method. The results agree well with the DFT results, as can be seen in Fig. 5. Based on a comparison with the DFT simulation of He migration [22], the new potential accurately describes He interstitial migration. A very low migration energy, E^m (He_{int}) = 0.065 eV, is found here for He with this three-dimensional mechanism, Such a low migration energy means that the migration of interstitial He is almost athermal.

Although there have been many interatomic potentials for Fe–He [4,5,20], the scheme in this work has features as followers. Our interatomic pair potential cover much larger phase space including not only the B1 phase, but also B3 structures. Second, the potential was derived directly from the total-energy difference between B1- and B3-type FeHe crystals, The potential functions could be selected in terms of the shapes of the inverted potential curves.

4. Conclusions

In this paper, we carried out density functional theory (DFT) based first principle calculations, using the projected augmented plane-wave (PAW) method in order to determine the total energies of two type FeHe crystals. The pair potentials for Fe–He was derived from total energies with multiple-lattice inversion techniques. Based on the potentials, we have applied MD method to examine this pair potential. Comparing with the *ab initio* calculation results, the stability of He-vacancy clusters at zero temperature and migration energy was well reproduced by this potential, indicating that the multiple-lattice inversion technique is useful and applicable to estimate the Metal-He potentials.

Acknowledgements

This work was supported in part by the Science and Technology Foundation of China Academy of Engineering Physics (Nos. 2009A0301019 and 2008A0301013).

References

[1] R.E. Stoller, J. Nucl. Mater. 174 (1990) 289.
[2] R. Vassen, H. Trinkaus, P. Jung, Phys. Rev. B 44 (1991) 4206.
[3] T. Seletskaia, Y.D. Osetskiy, R.E. Stoller, G.M. Stocks, J. Nucl. Mater. 367 (2007) 355.
[4] W.D. Wilson, in: Conference on Fundamental Aspects of Radiation Damage in Metals, USERDA-CONF-751006-P2, vol. 1025, 1975.
[5] N. Juslin, K. Nordlund, J. Nucl. Mater. 382 (2008) 143.
[6] M.J.L. Sangster, M.J. Norgett, J. Phys. C 10 (1977) 1395.
[7] M. Prencipe, A. Zupan, R. Dovesi, E. Apra, V. Saunders, Phys. Rev. B 51 (1995) 3391.
[8] C.R.A. Catlow, K.M. Diller, M.J. Norgett, J. Phys. C 10 (1977) 1395.
[9] A.E. Carlsson, C.D. Gelatt, H. Ehrenreich, Philos. Mag. A 41 (1980) 241.
[10] N.X. Chen, Z.D. Chen, Y.C. Wei, Phys. Rev. E 55 (1997) R5.
[11] N.X. Chen, N.X. Chen, X.J. Ge, W.Q. Zhang, F.W. Zhu, Phys. Rev. B 57 (1998) 14203.
[12] S. Zhang, N.X. Chen, Phys. Rev. B 66 (2002) 064106.
[13] G. Kress, J. Hafner, Phys. Rev. G 47 (1993) 558.
[14] G. Kress, J. Furthmuller, Phys. Rev. G 54 (1996) 11169.
[15] G. Kress, D. Joubert, Phys. Rev. G 59 (1999) 1758.
[16] J.P. Perdew, J.A. Chevary, S.H. Vosko, et al., Phys. Rev. B 46 (1992) 6671.
[17] H.J. Monkhorst, J.D. Pack, Phys. Rev. B 13 (1976) 5188.
[18] G.J. Ackland, D.J. Bacon, A.F. Calder, T. Harry, Philos. Mag. A 75 (1997) 713.
[19] R.A. Aziz, A.R. Janzen, M.R. Moldover, Phys. Rev. Lett. 74 (1995) 1586.
[20] T. Seletskaia, Y. Osetsky, R.E. Stoller, G.M. Stocks, J. Nucl. Mater. 351 (2006) 109.
[21] T. Seletskaia, Y. Osetsky, R.E. Stoller, G.M. Stocks, Phys. Rev. Lett. 94 (2005) 046403.
[22] C. Fu, F. Willaime, Phys. Rev. B 72 (2005) 064117.
[23] J.C. Hamilton, A.M. Foiles, Phys. Rev. B 65 (2002) 064104.
[24] H. Jonsson, G. Mills, G.K. Schenter, Surf. Sci. 324 (1995) 305.